J. Fluid Mech. (1983), *vol.* 132, *pp.* 105–118
Printed in Great Britain

Trapping of water waves above a round sill

By YURIKO RENARDY

Mathematics Research Center, University of Wisconsin–Madison,
610 Walnut Street, Madison, Wisconsin 53706

(Received 18 August 1981 and in revised form 14 January 1983)

The three-dimensional problem of wave trapping above a submerged round sill was first analysed by Longuet-Higgins on the basis of a linear shallow-water theory. The large responses predicted by the theory were, however, not well borne out by the experiments of Barnard, Pritchard & Provis, and this has motivated a more detailed study of the problem. A full linear theory for both inviscid and weakly viscous fluid, without any shallow-water assumptions, is presented here. It reveals important limitations on the use of shallow-water theory and the reasons for them. In particular, while the qualitative features of wave trapping are similar to those of shallow-water theory, the nearly resonant frequencies differ significantly, and, since the resonances are narrow, the observed amplitudes at a given frequency differ greatly. The geometry is strongly indicative of long waves, and the dispersion relation appears quite consistent with that, but the part of the motion at wavenumbers that are not small has, despite the small amplitude, a substantial effect on the response to excitation.

1. Introduction

A theoretical study of the trapping that results when a train of small-amplitude plane waves of a fixed frequency is incident on a submerged steep-sided round sill (figure 1) was made by Longuet-Higgins (hereinafter referred to as LH) in 1967. His investigation was motivated by wave records taken at Macquarie Island showing the occurrence of regular oscillations of unusually large amplitudes. In view of these observations, LH considered a simplified geometry in which the island shelf was represented by a round sill, with a circumference of 80 km, submerged to a depth of 100 m. He based his calculation on linear inviscid shallow-water theory, and used separation of variables in cylindrical coordinates to determine the expressions for the surface displacements for each of the two regions of constant depths. Because of the depth independence of the velocity field in shallow-water theory, the velocity components could not be made continuous at the sill edge, and two approximate matching conditions were used: the continuity of surface elevation and the continuity of the horizontal component of the mass flux. LH's analysis showed the existence of eigenfrequencies with very small imaginary parts. A train of plane waves with a frequency near such an eigenfrequency could theoretically excite 'nearly trapped' modes over the sill, and the response at such modes was determined. The largest responses were found to occur at the higher angular modes and at smaller ratios of the depths. These calculations have been confirmed and extended by Summerfield (1969), who applied shallow-water theory to a 'shelf–island' model consisting of a steep-sided round island rising from the top of a round sill of larger radius. He showed the eigenfrequencies for his system to be closely related to those of LH's sill geometry.

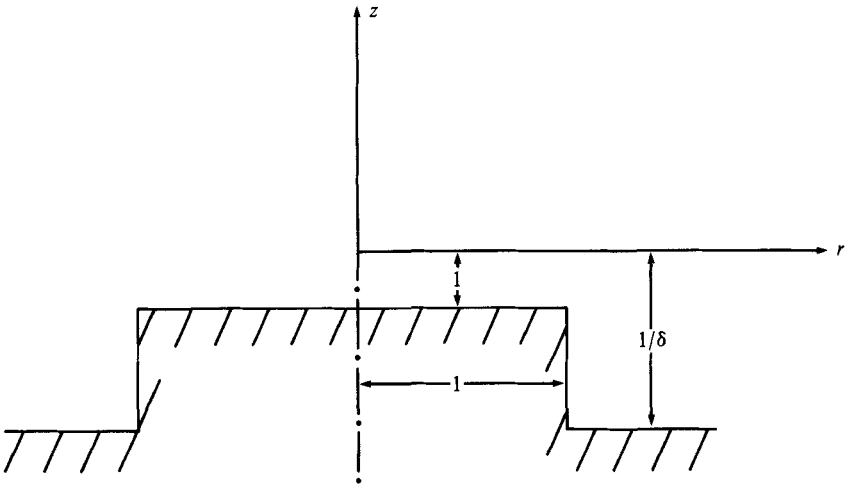

FIGURE 1

However, laboratory observations by Pite (1977) and by Barnard, Pritchard & Provis (1983, henceforth denoted by BPP) did not reveal the large responses predicted by the shallow-water model. The purpose of this paper is to examine a complete linear theory in an endeavour to explain these discrepancies.

In §2 the equations governing the full linear inviscid theory are presented. In §3 the velocity potential is calculated. This is achieved by representing it separately in the regions above the sill and outside the sill; the solutions in the two zones are then made to satisfy the necessary conditions of analytic continuation at the sill edge. This leads to an infinite set of linear equations, for which a collocation method of solution is described. In addition, an iterative method is presented as a check on the extensive calculations. No attempt has been made to account for separation effects at the sill edge. These effects could lead to additional damping.

In §4, the theory is applied to laboratory conditions relating to the experiments of BPP. The results show that the modes that decay away from the sill edge and are not included in shallow-water theory make appreciable contributions to the wave amplitudes above the sill. To obtain a comparison on oceanographic scales between the full theory and the shallow-water theory, the theoretical predictions for the special case of Longuet-Higgin's sill geometry are examined in §5. The differences are particularly striking near the frequencies where the full theory predicts large amplitudes, and the reasons for these differences are discussed. A theory allowing for weakly viscous effects is given in §6. Numerical computations were carried out at a frequency pertaining to the conditions considered by BPP. At that frequency, viscous effects were found to have negligible influence on the amplitudes. For the entire range of frequencies investigated by BPP, moreover, viscous effects are estimated to make less than 1% difference in the amplitudes, even at the frequencies where peak amplitudes are predicted. On oceanographic scales, however, where an eddy viscosity may be more appropriate than the kinematic viscosity, damping may be more pronounced.

2. General equations

The motion is assumed inviscid, simple-harmonic in time, and of sufficiently small amplitude for the use of linear theory. It is referred to cylindrical coordinates (r, θ, z) with the origin at the undisturbed water surface (see figure 1), r measured outward in units of the sill radius a, and z measured vertically upward in units of the undisturbed water depth d above the sill; the depth outside the sill is denoted by $D = d/\delta$. Let x denote the horizontal coordinate in the direction $\theta = 0$. A train of plane waves of frequency σ and amplitude $|\eta^*|_{\mathrm{I}}$ is incident on the sill from the positive x-axis. The surface displacement, measured in units of d, is denoted by η, and the velocity potential $\phi(r, \theta, z, t)$ is measured in units of $d^2\sigma$ and satisfies Laplace's equation, namely

$$\frac{\partial^2\phi}{\partial r^2}+\frac{1}{r}\frac{\partial\phi}{\partial r}+\frac{1}{r^2}\frac{\partial^2\phi}{\partial\theta^2}+\frac{a^2}{d^2}\frac{\partial^2\phi}{\partial z^2}=0, \tag{2.1}$$

together with the following boundary conditions: at the free surface $z = 0$

$$\eta_t = \sigma\phi_z,$$

$$\phi_{tt}+\frac{g}{d}\phi_z = 0 \quad (r \geqslant 0,\ 0 \leqslant \theta \leqslant 2\pi), \tag{2.2a}$$

on the horizontal portion of the seabed, $z = -1$ and $0 \leqslant r < 1$, and $z = -1/\delta, r > 1$

$$\phi_z = 0, \tag{2.2b}$$

and on the vertical wall of the sill at $r = 1$, $-1/\delta < z < 1$

$$\phi_r = 0. \tag{2.2c}$$

At large distances from the sill, the wave-field is assumed to consist of the incident wave, whose surface elevation is the real part of

$$\eta_{\mathrm{I}} = |\eta|_{\mathrm{I}} e^{-\mathrm{i}(Kx+\sigma t)},$$

together with waves that either decay or radiate outwards. Here K is the positive real root of the dispersion relation

$$\frac{KD}{a}\tanh\frac{KD}{a} = \frac{D\sigma^2}{g}. \tag{2.3}$$

Different representations of the solution will be used in the domain above the sill, $r < 1$, and in that outside the sill, $r > 1$. These functions must be analytic continuations of each other, for which a necessary and sufficient condition is the continuity of ϕ and $\partial\phi/\partial r$.

3. Form of solutions

Let the velocity potentials for $r < 1$ and $r > 1$ be denoted by ϕ_{s} and ϕ_0 respectively, and be simple harmonic in time with radian frequency σ. Make the decomposition $\phi_0 = \phi_{\mathrm{I}}+\phi_{\mathrm{R}}$, where ϕ_{I} represents the incident plane wavetrain and ϕ_{R} represents waves generated by the sill. ϕ_{I} is calculated by separation of variables in Cartesian coordinates:

$$\phi_{\mathrm{I}} = \tfrac{1}{2}|\eta|_{\mathrm{I}} e^{-\mathrm{i}(a\lambda_0 x/D+\sigma t)}\frac{\cosh\lambda_0(\delta z+1)}{\lambda_0\sinh\lambda_0}+*. \tag{3.1}$$

Here, and throughout the paper, the notation $+*$ will be used to denote the addition of the complex conjugate of all preceding terms. The free-surface boundary conditions require λ_0 to be the real and positive root of the dispersion relation (see e.g. Davis & Hood 1976)

$$\lambda \tanh \lambda = \frac{D\sigma^2}{g}. \tag{3.2}$$

For convenience, the expression for ϕ_I is converted to cylindrical coordinates (Erdélyi *et al.* 1953, §7.2.4):

$$\phi_I = e^{-i\sigma t} \frac{\cosh \lambda_0(\delta z+1)}{2\lambda_0 \sinh \lambda_0} \sum_{m=0}^{\infty} \epsilon_m i^{-m} J_m\left(\frac{a\lambda_0 r}{D}\right) \cos m\theta + *, \tag{3.3}$$

where $\epsilon_0 = 1$ and $\epsilon_m = 2$ $(m \neq 0)$. For the purpose of computations for the linearized problem, $|\eta|_I$ is normalized to unity.

The generated field in the region outside the sill, $r > 1$, may be represented as the sum (Havelock 1929)

$$\phi_R = e^{-i\sigma t} \sum_{m=0}^{\infty} \cos m\theta \left\{ B_{m0} H_m^{(1)}\left(\frac{a\lambda_0 r}{D}\right) \cosh \lambda_0(\delta z+1) + \sum_{n=1}^{\infty} B_{mn} K_m\left(\frac{a\lambda_n r}{D}\right) \frac{\cos \lambda_n(\delta z+1)}{K_m(a\lambda_n/D)} \right\} + *. \tag{3.4}$$

Here elements of $\{\pm i\lambda_m : m = 1, 2, \ldots\}$ are the purely imaginary roots of the dispersion relation (3.2). Note that the modal expansion is complete (Davis & Hood 1976) and that $\lambda_m = m\pi$ for m sufficiently large or for $D\sigma^2/g$ sufficiently small. The notations for the Bessel functions are those of Abramowitz & Stegun (1972). Each term in (3.4) satisfies the appropriate conditions at infinity as well as the free-surface conditions and boundary conditions on the seabed. The coefficients B_{m0} and B_{mn} $(n \neq 0)$, as yet undetermined, are respectively coefficients of each radiating mode and each non-radiating mode, which is confined near the sill edge. From now on, the subscript on λ_0 and the superscript on the Hankel function will be dropped.

The solution in the sill region, $r < 1$, may be represented as the sum of solutions obtained by separation of variables, namely

$$\phi_s = e^{-i\sigma t} \sum_{m=0}^{\infty} \cos m\theta \left\{ A_{m0} J_m\left(\frac{akr}{d}\right) \cosh k(z+1) + \sum_{n=1}^{\infty} A_{mn} I_m\left(\frac{ak_n r}{d}\right) \cos k_n(z+1) \Big/ I_m\left(\frac{ak_n}{d}\right) \right\} + *. \tag{3.5}$$

Here elements of $\{k_0, ik_n : n = 1, 2 \ldots\}$ are the roots of

$$k \tanh k = \frac{d\sigma^2}{g}, \tag{3.5a}$$

of which each of the k_n are positive. Each term satisfies the appropriate conditions at the edge of the sill, at the free surface and on the seabed. The, as yet undetermined, coefficients A_{m0} and A_{mn} $(n \neq 0)$ are respectively coefficients of each wavelike mode and each spatially decaying mode. In what follows, the subscript on k_0 will be dropped.

The continuity of $\partial\phi/\partial r$ at $r = 1$, $-1 < z < 0$, $0 \leqslant \theta \leqslant 2\pi$ yields one of the

two conditions at the sill edge:

$$\frac{\partial \phi_0}{\partial r} = \begin{cases} \dfrac{\partial \phi_s}{\partial r} & (-1 < z < 0), \\ 0 & (-1/\delta < z < -1). \end{cases} \tag{3.6}$$

By virtue of the orthogonality property of the set

$$\{\cosh\lambda(\delta z+1),\ \cos\lambda_n(\delta z+1)\colon n = 1, 2, \ldots\},$$

this condition yields, for $m = 0, 1, \ldots,$

$$\left[B_{m0}H'_m\left(\frac{a\lambda}{D}\right)+F^*_m\right]\frac{a\lambda}{D}h(\lambda) = \int_{-1}^{0}\left.\frac{\partial\phi_m}{\partial r}\right|_{r=1}\cosh\lambda(\delta z+1)\,\mathrm{d}z. \tag{3.7a}$$

Here ϕ_m denotes the coefficient of $\cos m\theta\, \mathrm{e}^{-\mathrm{i}\sigma t}$ in ϕ_s, and F^*_m and $h(\lambda)$ are defined in the appendix. For $n = 1, 2, \ldots,$

$$B_{mn}\frac{K'_m(a\lambda_n/D)}{K_m(a\lambda_n/D)}\frac{a\lambda_n}{D}h(\mathrm{i}\lambda_n) = \int_{-1}^{0}\left.\frac{\partial\phi_m}{\partial r}\right|_{r=1}\cos\lambda_n(\delta z+1)\,\mathrm{d}z. \tag{3.7b}$$

At the edge of the sill ($r = 1$, $z = -1$, $0 \leqslant \theta \leqslant 2\pi$), there is a singularity in $\mathrm{d}\phi/\mathrm{d}r$. However, since it behaves locally like $r^{-\frac{1}{3}}$, the integrations in (3.7*a*, *b*) are possible.

The second condition at $r = 1$, $-1 < z < 0$, $0 \leqslant \theta \leqslant 2\pi$ is the continuity of ϕ. This yields a second relation between B_{mn} and A_{mn}, from which the B_{mn} are eliminated by means of (3.7*a*, *b*). The resulting equations for the A_{mn} are

$$A_{m0}\left\{\cosh k(z+1)\,J_m\left(\frac{ak}{d}\right)-l_{m0}(z)\right\}+\sum_{p=1}^{\infty}A_{mp}\{\cos k_p(z+1)-l_{mp}(z)\}$$

$$=\left\{F_m-F^*_m\frac{H_m(a\lambda/D)}{H'_m(a\lambda/D)}\right\}\cosh\lambda(\delta z+1) \quad (-1 < z < 0,\ m = 0, 1, \ldots). \tag{3.8}$$

The notation is defined in the appendix. When no spatially decaying modes are included (3.8) is first multiplied by $\cosh k(z+1)$ and then integrated over z. With the inclusion of the decaying modes, a collocation method is used to solve the resulting infinite number of equations: that is, an $N \times N$ matrix equation is constructed by the application of (3.8) at N values of z in the range $-1 < z < 0$ and by neglecting the higher-order decaying modes $\{A_{mp}\colon p \geqslant N\}$. The function involved in this collocation scheme is ϕ, which behaves like $r^{\frac{2}{3}}$ at the sill edge. Thus, although the radial velocity is infinite at the edge, this scheme converges.

Justification for the matrix truncation, which is performed in the calculations of the following sections, is as follows. For the investigation on the laboratory scales described in §4, the N values of z were chosen to be $\{z\colon z = -i/(N+1), i = 1, \ldots, N\}$ for $N = 2, 6, 11, 16, 21, 41$. It is shown in §4 that the differences in the resulting amplitudes for $N \geqslant 6$ was of negligible importance. Hence it is apparent that the above choice for the values of z, with $N = 6$, was adequate for computations involving similar sill geometries. The computations in §5 concern scales for which the parameter a/d was much greater than in §4, so that the local modes decayed faster away from the sill edge than those of §4. Since experimental results by Pite (1977) and, independently, by BPP indicated almost no presence of exponential decay in the wave field near the sill edge, it is expected that the faster the local modes decay, the less will be their response. Therefore $N = 6$, which was sufficiently accurate for §4, was

also expected to give suitable accuracy for §5, and has also been used for the computations described in §5.

The computations are made difficult by the presence, in (3.8), of the infinite series in the terms $l_{mp}(z)$ for $p = 0, 1, \ldots, m = 0, 1, \ldots$, which are slowly convergent. Because of this, a numerical check on the complicated computations was required, and an iterative method is now presented for this purpose.

The decomposition of ϕ_s in the radial variable yields (as shown by (3.5)) a principal part $J_m(akr/d)$, which is wavelike, and an infinite number of modes $I_m(ak_n r/d)$ that decay away from the sill edge. If the value of the principal radial eigenfunction at the sill edge is not too small, then an iterative procedure may be adopted. From now on, the coefficient of $\cos m\theta\, e^{-i\sigma t}$ in ϕ_s and ϕ_0 will be denoted by ϕ_m.

A preliminary outer flow is determined from the radiation condition and the boundary condition $\partial\phi_m/\partial r = 0$ at $r = 1$, $-1 < z < 0$. This outer flow then determines the boundary condition at $r = 1$, $-1 < z < 0$, for a sill flow, through the continuity of ϕ. This sill flow then yields $\partial\phi_m/\partial r$ at $r = 1$, $-1 < z < 0$, from which a second outer flow is calculated, and so forth.

Equations (A 1) and (A 2) in the appendix arise from this scheme and are to be used as follows. When the A_{mn} in ϕ_s are known, the coefficients B_{mn} of ϕ_0 are calculated from (A 1). Note that here $H'_m(a\lambda/D)$, $I_m(ak_n/d)$ and $K'_m(a\lambda_p/D)$ do not vanish. When the B_{mn} are known, the coefficients in ϕ_s are calculated from (A 2). This iteration diverges near the zeros of $J_m(ak/d)$, which lie near the peak periods. This scheme therefore fails for the parameters of most interest, but it was felt important to use the method to provide a check on the computations made with (3.8).

4. Application to laboratory scales

This section concerns some calculations made to correspond to the laboratory scales used by BPP. For their experiments, $a = 50$ cm, $d = 1.75$ cm, $D = 15.4$ cm, and the forcing periods ranged between 0.75 and 1.20 s.

The full linear theory with no spatially decaying modes was used to compute the response curve for each model number and were compared with the linear shallow-water theory. Figures 2 (a, b) display the results for the 0th mode and figure 3 those of the 6th mode. The curves show that the peaks in the lower frequency range occurred near those of linear shallow-water theory. At small modal numbers, however, the response was significantly diminished, and at large modal numbers the bandwidths were small so that Longuet-Higgins' theory was not useful in calculations of the amplitudes. In the higher frequency range, there was no evidence of the peaked response predicted by the LH theory. In this connection, note that there are a large number of zeros in the radial eigenfunction $J_m(akr/d)$ in the sill region. Thus the horizontal scale of the motion is so much smaller than the radius that the motion is not a long wave, and this is the most probable source of the substantial error in that theory.

Computations, accounting also for the decaying modes, were carried out at the forcing period of 1.181 s where the measurements by BPP yielded the largest amplitude above the sill. The difference between the empirical values $(|\eta_E(r_i, \theta_j)| : r_i = \frac{1}{14} + \frac{1}{7}(i-1), i = 1, \ldots, 7, \theta_j = \frac{1}{18}(j-1), j = 1, \ldots, 19)$ and the theoretical values $(|\eta_T|)$ of the wave amplitudes was measured by

$$E_2 = \left[\frac{\sum_{i=1}^{7} \sum_{j=1}^{19} w_{ij} [|\eta_E(r_i, \theta_j)| - |\eta_T(r_i, \theta_j)|]^2 r_i}{\sum_{i=1}^{7} \sum_{j=1}^{19} w'_{ij} |\eta_E(r_i, \theta_j)|^2 r_i} \right]^{\frac{1}{2}}, \tag{4.1}$$

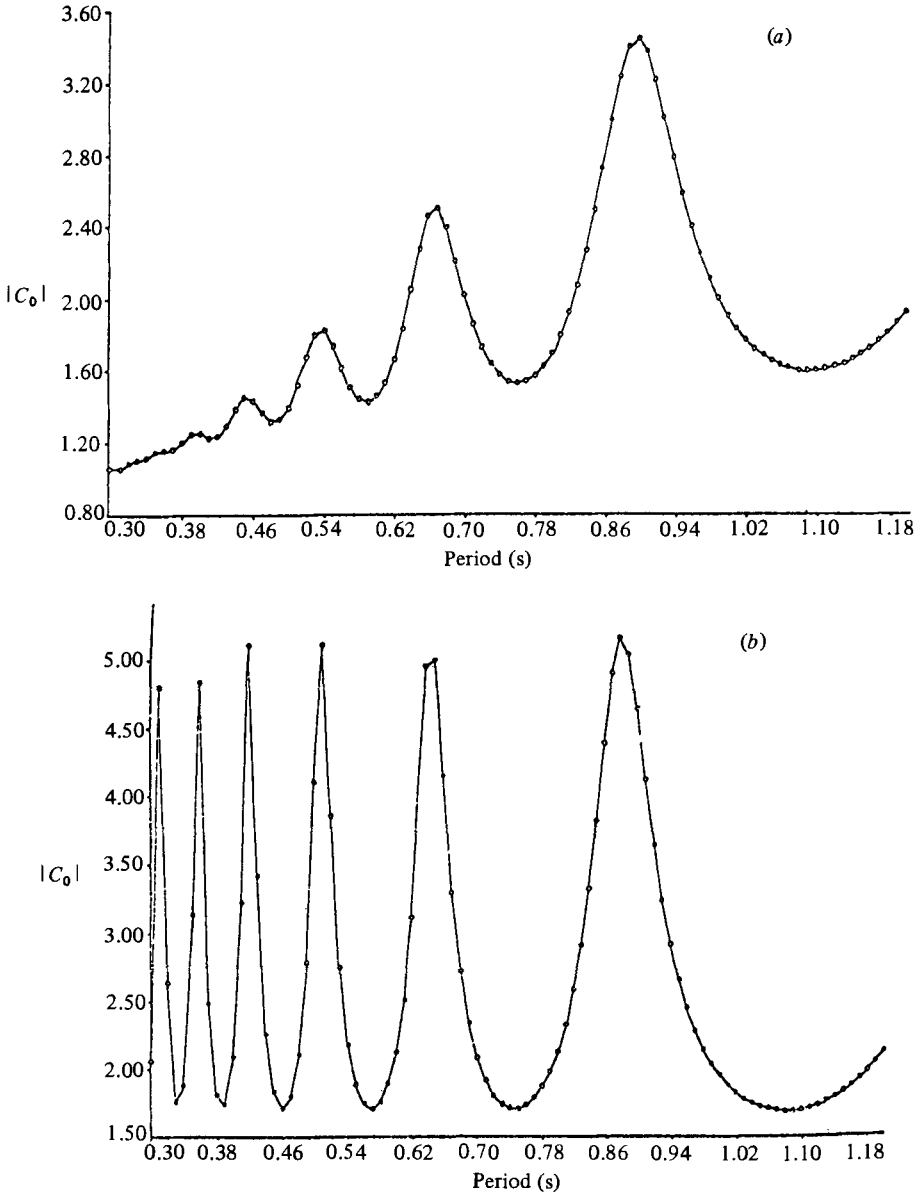

FIGURE 2. (*a*) Linear-theory response with no 'decaying' modes, for the BPP sill; modenumber 0. (*b*) Linear shallow-water response, $|C_0|$ versus period, for the BPP sill; modenumber 0.

$$E_{\mathrm{m}} = \frac{\max\limits_{i,j} |\,|\eta_{\mathrm{E}}(r_i, \theta_j)| - |\eta_{\mathrm{T}}(r_i, \theta_j)|\,|}{\max\limits_{i,j} |\eta_{\mathrm{E}}(r_i, \theta_j)|}. \tag{4.2}$$

The coefficients w_{ij} and w'_{ij} represent the weights determined by Simpson's rule for integration over θ $(0 \leqslant \theta \leqslant \pi)$ and r $(r_1 \leqslant r \leqslant r_7)$, together with additional terms from the integration over $0 \leqslant r \leqslant r_1$ and $r_7 \leqslant r \leqslant 1$. For example, the square of the numerator of E_2 is

$$\tfrac{1}{21}\{S(r_1)\,r_1 + S(r_7)\,r_7 + 4(S(r_2)\,r_2 + S(r_4)\,r_4 + S(r_6)\,r_6) + 2(S(r_3)\,r_3 + S(r_5)\,r_5)\}$$
$$+ \tfrac{1}{14}(S(r_1)\,r_1 + S(r_7)\,r_7), \tag{4.3}$$

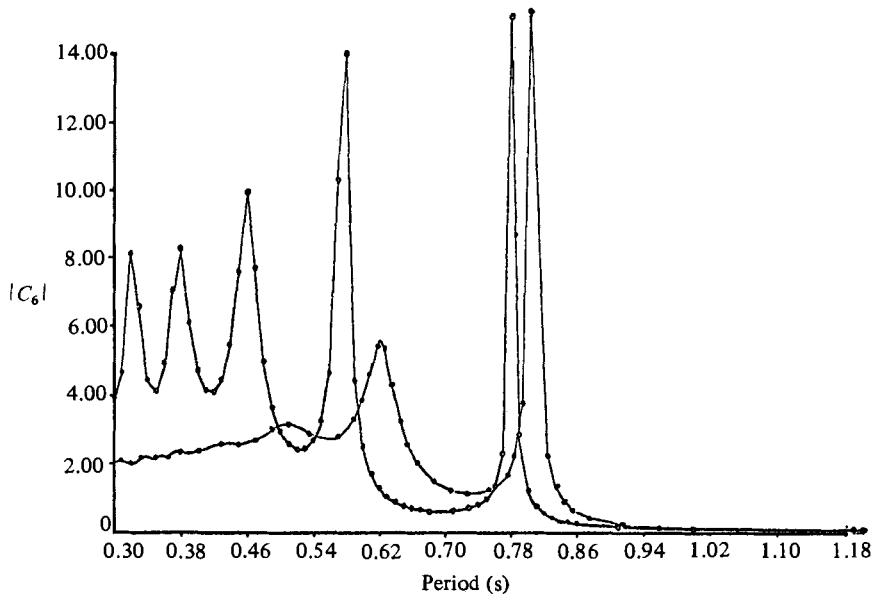

FIGURE 3. ---○---, linear shallow-water response, $|C_6|$ versus period, for the BPP sill; modenumber 6. ---○---, linear response, $|C_6|$ versus period with no decaying modes, for the BPP sill.

where, for $i = 1,\ldots,7$,

$$S(r_1) = \tfrac{1}{54}\pi\{4 \sum_{j=2n,\ n=1,\ldots,9} (|\eta_E(r_i,\theta_j)| - |\eta_T(r_i,\theta_j)|)^2$$

$$+2 \sum_{j=2n+1,\ n=1,\ldots,8} (|\eta_E(r_i,\theta_j)| - |\eta_T(r_i,\theta_j)|)^2$$

$$+ (|\eta_E(r_i,\theta_1)| - |\eta_T(r_i,\theta_1)|)^2 + (|\eta_E(r_1,\theta_{19})| - |\eta_T(r_i,\theta_{19})|)^2\}. \tag{4.4}$$

A consistency check on E_2 was made by using the w_{ij} and w'_{ij} according to the midpoint rule.

When only the travelling modes A_{m0} ($m = 0,\ldots,8$) were included in the computations, the improvement in E_2 over the LH theory was from 55 % to 47 %. When the first decaying mode A_{m1} ($m = 0,\ldots,8$) was included, together with a large number of 'outer' decaying modes, E_2 was further improved from 47 % to 35 %. With the inclusion of from 5 to 40 'sill' decaying modes, E_2 decreased by negligible amounts. These results document the importance of the decaying modes, which had previously been thought negligible (Pite 1977).

The above computational results are explained as follows. The experimental conditions may be modelled by the full equation (3.8) when δ and $D\sigma^2/g$ are both small. Under these conditions, the response equation becomes approximately

$$A_{m0}\left\{J_m(ak/d) - kJ'_m(ak/d)\left(\frac{H_m(a\lambda/D)}{\lambda H'_m(a\lambda/D)} + X + Y\right)\right\} = F_m - F_m^* \frac{H_m(a\lambda/D)}{H'_m(a\lambda/D)}, \tag{4.5}$$

where

$$X = \frac{-2}{\pi^3\delta^2} \sum_{n=1}^{\infty} \frac{\sin^2 n\pi(1-\delta)}{n^3}, \quad Y = \frac{8}{\pi^5} \sum_{p=1}^{\infty} p \sum_{n=1}^{\infty} \frac{\sin^2 \nu\pi(1-\delta)^2}{n(n^2\delta^2 - p^2)}.$$

X is $O(1/\delta^2)$ and originates from the 'outer' decaying modes, of which a large number must be included in the computations. Y is $O(1)$ and originates from the 'sill'

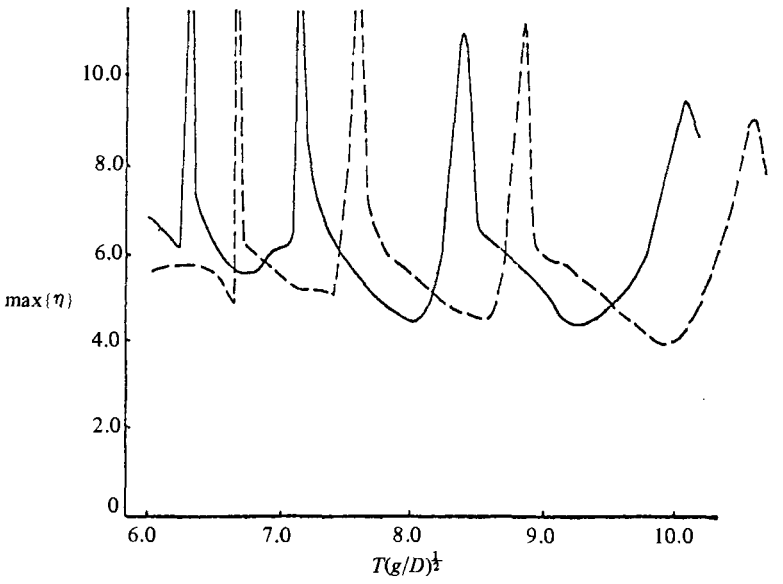

FIGURE 4. Max$\{\eta\}$ as a function of $T(g/D)^{\frac{1}{2}}$. ———, full linear theory; ——-, LH shallow-water theory.

decaying modes. Equation (4.5) indicates that the inclusion of the 'outer' decaying modes is crucial to the satisfaction of the sill-edge conditions, but that the inclusion of the 'sill' decaying modes is not. This accounts for the differences in E_2 described in the last paragraph.

The maximum amplitudes above the sill and the amount of mechanical energy over the sill were computed using the full linear theory with 5 'sill' decaying modes. The results, for the experimental range of forcing frequencies, are shown in figures 4 and 5 together with those of the LH theory. Compared with the peaks given by the LH theory for this range of frequencies, those of the full linear theory were shifted significantly to higher periods, with increased magnitude in the case of the 'energy' graph. The peaks of the full linear theory occur near the complex zeros of the coefficient of A_{m0} in (4.5). The LH theory peaks near the zeros k of

$$J_m(ak/d) - \frac{kJ'_m(ak/d)\,H_m(a\lambda/D)}{\lambda H'_m(a\lambda/D)} = 0,$$

where $k^2 = d\sigma^2/g = \delta\lambda^2$. This indicates that the shifts arise through the term $X+Y$, which is $O(1/\delta^2)$ for small δ. The LH theory is therefore useful here only when $k/\delta^2 \ll 1$. If ak/d is too small, however, there is no resonance in the system. This indicates that the linear shallow-water theory is useful if $D\sigma^2/g$ and k/δ^2 are both small and ak/d is not small.

It appears therefore that a shallow-water theory is not necessarily a good approximation to the full linear theory even though the boundary conditions seem to indicate it. The reason lies in the extreme sensitivity of the matrix equation arising from (3.8) (and hence the response) to what might be presumed to be small perturbations. For example, the terms arising from the decaying modes might at first guess be thought to be unimportant; indeed, their relative excitations A_{mp}/A_{m0} for $p = 1, 2, \ldots, m = 0, 1, \ldots$ can be shown to be small. Also, the wavenumbers k and λ, when evaluated by the full linear dispersion relations, differed only slightly from their

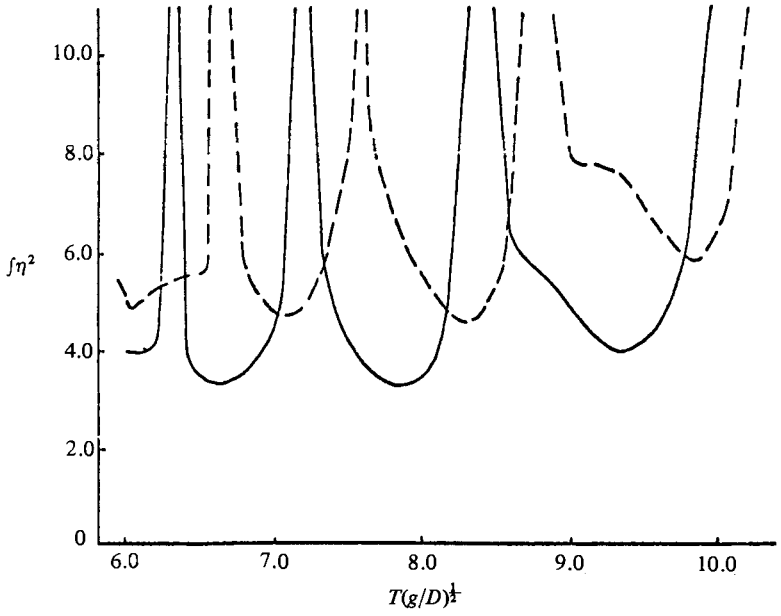

FIGURE 5. A graph of $\int \eta^2$ as a function of $T(g/D)^{\frac{1}{2}}$: ———, full linear theory; ——, LH shallow-water theory.

shallow-water values. Their small differences, however, caused noticeable effects on (3.8) through the Bessel functions, especially at forcing frequencies at which the resulting matrix equation was nearly singular, and these are just the frequencies of peak response. The standard, diagnostic checks on dispersion relation and modal amplitudes do turn out to mislead.

An implication of this result is that shallow-water theory should be used only with great care in interpreting experimental results concerning motions that in theory exhibit sharp changes in the response for small changes in the forcing. Another is that great care may need to be taken with the numerical work at such frequencies.

5. Application to oceanographic scales

Longuet-Higgins (1967) calculated the response $|A_n|$, where

$$\eta = \sum_{-\infty}^{\infty} e^{i(n\theta-\sigma t)} A_n J_n(ak_1 r), \quad k_1 = \frac{\sigma}{(gd)^{\frac{1}{2}}},$$

for a selection of frequencies. The corresponding response using the full linear theory is $|C_{m0}|/\epsilon_m$, where

$$\eta = e^{-i\sigma t} \sum_{m=0}^{\infty} \cos m\theta \left[C_{m0} J_m(akr/d) + \sum_{n=1}^{\infty} C_{mn} \frac{I_m(ak_n r/d)}{I_m(ak_n/d)} \right] + *,$$

$$C_{m0} = A_{m0}\left(\frac{id\sigma^2}{g}\right) \cosh k \quad (m = 0, 1, \ldots),$$

$$C_{mn} = A_{mn}\left(\frac{id\sigma^2}{g}\right) \cos k_n \quad (m = 0, 1, \ldots, \ n = 1, 2, \ldots).$$

Mode no.	Dimensionless frequency $\frac{a\sigma}{(gd)^{\frac{1}{2}}}$	Longuet-Higgins' $\lvert A_n \rvert$	Full linear theory's coefficient of travelling mode
	$\delta = \frac{1}{16}$		
2	4.921	16.23	11.88
	8.219	8.057	7.267
4	7.447	91.37	2.145
	10.798	18.90	5.756
	14.027	8.593	6.233
6	9.821	581.1	0.2798
	13.408	85.81	1.176
	16.723	24.21	2.840
	19.922	10.42	4.331
	23.235	7.122	4.196
8	12.121	3895	0.0757
	15.890	437.8	0.2235
	19.352	98.12	0.7472
	22.662	31.76	1.714
	25.869	13.55	2.797
	29.083	7.954	3.269
	32.480	6.512	2.769
	$\delta = \frac{1}{4}$		
2	4.796	2.871	2.775
3	5.632	3.269	2.921
4	6.799	3.546	3.526
5	8.021	4.447	4.482
6	9.240	5.841	5.644
	12.832	3.738	2.516
8	11.630	10.83	5.351
	15.025	3.018	3.026
	$\delta = \frac{9}{16}$		
5	6.8903	0.978	1.357
6	8.124	1.158	1.447
7	9.308	1.296	1.531

TABLE 1. Comparison of full linear theory with Longuet-Higgins' (1967) response $|A_n|$ in the surface elevation

The results for the frequencies and depth ratios δ considered by LH are listed in table 1. For $\delta = \frac{9}{16}$ there were not very large differences between the predictions of the two theories. At $\delta = \frac{1}{16}$, however, the LH theory predicted very large responses, especially at larger values of m. The matrix equation was then sensitive to approximations inherent in shallow-water theory, mentioned toward the end of §4, and the two theories produced very different results.

It is of interest to delineate the parameter ranges for which the shallow-water theory may be useful. This theory is based on the smallness of the parameter $D\sigma^2/g$ and the practical range for which the theory appears to be useful is limited to values of this parameter rather less than 0.1 (Silvester 1974, table 4.1). On the other hand,

the dimensionless frequencies $a\sigma/(gd)^{\frac{1}{2}}$ at which resonance occurs lie close to the zeros of $J_m(z)$; the smallest zeros of $J_m(z)$ increase as m increases, and for m greater than 6 the first zeros are greater than 10. Since the shallow-water parameter is related to $a\sigma/(gd)^{\frac{1}{2}}$ by $D\sigma^2/g = (a\sigma/(gd)^{\frac{1}{2}})^2\,(d/a)^2/\delta$, the LH theory is likely to be useful for an appropriate combination of (i) d/a small, (ii) δ not too small, and (iii) m not too large. The large, narrow, 'resonant' peaks predicted by the LH theory, however, occurred for parameter ranges not satisfying these restrictions. For instance, table 1 ($d/a \approx 0.008$) shows that the most spectacular peaks occurred for larger m and smaller δ and that these peaks were not predicted by the more accurate linear theory.

6. Weakly viscous effects

Consider a periodic flow above the sill at a frequency σ. At the solid boundary there will be a Stokes boundary layer of thickness $(\nu/\sigma)^{\frac{1}{2}}$, where ν is the kinematic viscosity of the fluid. For laboratory scales, ν is assumed to be 0.01 $\mathrm{cm^2\ s^{-1}}$ (for water) and for the field scales, ν may be the eddy viscosity, perhaps of the order of 10 $\mathrm{cm^2\ s^{-1}}$. In the sill geometry of BPP, $(\nu/\sigma)^{\frac{1}{2}}/d = 0.05$, and, for the case considered by LH, this parameter was an order of magnitude smaller. The effect of viscous dissipation at the bottom boundary outside the sill region is expected to be small compared with that inside. In order to estimate the effect of viscosity on the total flow, it is therefore plausible to take the boundary layer into account for $r < 1$, and to neglect it for $r > 1$. Following the work of Mahony and Pritchard (1980) the boundary condition to be posed at $z = -1$, $r < 1, 0 \leqslant \theta \leqslant 2\pi$ is found to be

$$\frac{\partial \phi}{\partial z} = -\epsilon_1 e^{\frac{1}{4}i\pi} \frac{\partial^2 \phi}{\partial z^2} + O(\epsilon_1^3 \epsilon_2^4),$$

where $\epsilon_1 = (\nu/\sigma)^{\frac{1}{2}}/d$ and $\epsilon_2 = (d/a)^2$.

Computations for the sill geometry studied by BPP showed approximately a 1 % difference in E_2 (as defined by 4.1)) from the inviscid case, over the entire frequency range. Thus it would appear that the effect of viscosity is not important under their conditions. The suggestion by Pite (1977), who used a quasi-empirical theory that involves a fluctuating body force, that viscous effects were significant on his laboratory scales, does not appear to be justifiable since his values of ϵ_1 and ϵ_2 were similar to those of BPP.

The author is indebted to Professor J. J. Mahony (University of Western Australia) for suggesting this topic and for many helpful discussions. Thanks are also due to Dr W. G. Pritchard (University of Essex) for suggestions involving §4 and for help in drafting this paper, and to Professor R. E. Meyer (University of Wisconsin–Madison) for advice on the presentation.

The work for this paper was supported in part by a Commonwealth Post-graduate Research Award, by National Science Foundation Grant no. MCS-7927062 and by U.S. Army Contract no. DAAG29-80-C-0041.

Appendix

$$\epsilon_m = \begin{cases} 1 & (m = 0), \\ 2 & (m \neq 0), \end{cases}$$

$$f(k) = \int_{-1}^{0} \cosh^2 k(z+1)\,\mathrm{d}z,$$

$$F_m = \frac{\epsilon_m \mathrm{i}^{-m} J_m\left(\frac{a\lambda}{D}\right)}{2\lambda \sinh \lambda}, \quad F_m^* = \frac{\epsilon_m \mathrm{i}\, J'_m\left(\frac{a\lambda}{D}\right)}{2\lambda \sinh \lambda},$$

$$g(\lambda, k) = \int_{-1}^{0} \cosh \lambda(z+1) \cosh k(z+1)\,\mathrm{d}z, \quad h(\lambda) = \int_{-1/\delta}^{0} \cosh^2 \lambda(\delta z+1)\,\mathrm{d}z,$$

$$H_m\left(\frac{a\lambda}{D}\right) = H_m^{(1)}\left(\frac{a\lambda}{D}\right), \quad H'_m\left(\frac{a\lambda}{D}\right) = H_m^{(1)\prime}\left(\frac{a\lambda}{D}\right),$$

$$l_{mp}(z) = \begin{cases} \dfrac{kJ_m\left(\frac{ak}{d}\right)}{\delta}\left[\dfrac{\cosh \lambda(\delta z+1)}{\lambda h(\lambda)} \dfrac{H_m\left(\frac{a\lambda}{D}\right)}{H'_m\left(\frac{a\lambda}{D}\right)} g(\lambda, k) \right. \\ \qquad \left. + \sum_{n=1}^{\infty} \dfrac{K_m\left(\frac{a\lambda_n}{D}\right)}{K'_m\left(\frac{a\lambda_n}{D}\right)} \dfrac{\cos \lambda_n(\delta z+1)}{\lambda_n h(\mathrm{i}\lambda_n)} g(\mathrm{i}\lambda_n, k)\right] & (p = 0), \\ \dfrac{k_p}{\delta} \dfrac{I'_m\left(\frac{ak_p}{d}\right)}{I_m\left(\frac{ak_p}{d}\right)}\left[\dfrac{\cosh \lambda(\delta z+1)}{\lambda h(\lambda)} \dfrac{H_m\left(\frac{a\lambda}{D}\right)}{H'_m\left(\frac{a\lambda}{D}\right)} g(\lambda, \mathrm{i}k_p) \right. \\ \qquad \left. + \sum_{n=1}^{\infty} \dfrac{K_m\left(\frac{a\lambda_n}{D}\right)}{K'_m\left(\frac{a\lambda_n}{D}\right)} \dfrac{\cos \lambda_n(\delta z+1)}{\lambda_n(\mathrm{i}\lambda_n)} g(\mathrm{i}\lambda_n, \mathrm{i}k_p)\right] & (p \neq 0). \end{cases}$$

$$B_{m0} = \frac{1}{H'_m\left(\frac{a\lambda}{D}\right)}\left\{\frac{1}{\delta\lambda h(\lambda)}\left[kA_{m0} g(\lambda, k) J'_m\left(\frac{ak}{d}\right) + \sum_{n=1}^{\infty} k_n A_{mn} \frac{I'_m\left(\frac{ak_n}{d}\right)}{I_m\left(\frac{ak_n}{d}\right)} g(\lambda, \mathrm{i}k_n)\right] - F_n^*\right\}$$
$$(m = 0, 1, \ldots), \quad \text{(A 1}a\text{)}$$

$$B_{mp} = \frac{K_m\left(\frac{a\lambda_p}{D}\right)}{K'_m\left(\frac{a\lambda_p}{D}\right)} \delta\lambda_p h(\mathrm{i}\lambda p)\left\{kA_{m0} g(\mathrm{i}\lambda_p, k) J'_m\left(\frac{ak}{d}\right) + \sum_{n=1}^{\infty} k_n A_{mn} \frac{I'_m\left(\frac{ak_n}{d}\right)}{I_m\left(\frac{ak_n}{d}\right)} g(\mathrm{i}\lambda_p, \mathrm{i}k_n)\right\}$$
$$(p = 1, 2, \ldots). \quad \text{(A 1}b\text{)}$$

$$A_{m0} = \frac{1}{J_m(ak/d) f(k)}\left\{\left[B_{m0} H_m\left(\frac{a\lambda}{D}\right) + F_m\right] g(\lambda, \kappa) + \sum_{n=1}^{\infty} B_{mn} g(\mathrm{i}\lambda_n, k)\right\} \quad (m = 0, 1, \ldots),$$
$$\text{(A 2}a\text{)}$$

where $f(k)$, F_m and $g(\lambda, k)$ are defined above;

$$A_{mp} = \frac{1}{f(\mathrm{i}k_p)}\left\{\left[B_{m0}H_m\left(\frac{a\lambda}{D}\right)+F_m\right]g(\lambda,\mathrm{i}k_p)+\sum_{n-1}^{\infty}B_{mn}g(\mathrm{i}\lambda_n,\mathrm{i}k_p)\right\} \quad (p=1,2,\ldots). \tag{A 2b}$$

REFERENCES

ABRAMOWITZ, M. & STEGUN, I. A. (eds.) 1972 *Handbook of Mathematical Functions*. Washington: Natl. Bur. Stand.

BARNARD, B., PRITCHARD, W. G. & PROVIS, D. 1983 *Geophys. Astrophys. Fluid Dyn* (to appear).

CHURCHILL, R. V. 1963 *Fourier Series and Boundary-Value Problems*. McGraw-Hill.

CHURCHILL, R. V. 1972 *Operational mathematics*. McGraw-Hill.

DAVIS, A. M. & HOOD, M. J. 1976 Surface waves normally incident on a submerged horizontal cylinder. *SIAM J. Appl. Maths* **31**, 28.

ERDÉLYI, A., MAGNUS, W., OBERHETTINGER, F. & TRICOMI, F. G. 1953 *Higher Transcendental Functions*, vol. 2. McGraw-Hill.

HAVELOCK, T. H. 1929 Forced surface-waves on water. *Phil. Mag.* **8**(7), 569–576.

LONGUET-HIGGINS, M. S. 1967 On the trapping of wave energy round islands. *J. Fluid Mech.* **29**, 781–821.

MAHONY, J. J. & PRITCHARD, W. G. 1980 Wave reflexion from beaches. *J. Fluid Mech.* **101**, 809–832.

MEYER, R. E. 1971 Resonance of unbounded water bodies. In *Mathematical Problems in the Geophysical Sciences* (ed. W. H. Reid). Lecture Notes in Mathematics, vol. 13, pp. 189–227. Am. Math. Soc., Providence, Rhode Island.

MEYER, R. E. 1979 Theory of water-wave refraction. *Adv. Appl. Mech.* **19**, 53–141.

PHILLIPS, O. M. 1966 *The Dynamics of the Upper Ocean*. Cambridge University Press.

PITE, H. D. 1977 The excitation of damped waves diffracted over a submerged circular sill. *J. Fluid Mech.* **82**, 621–641.

RABINOWITZ, P. & DAVIS, P. J. 1975 *Methods of Numerical Integration*. Academic.

SILVESTER, R. 1974 *Coastal Engineering*, 1. Elsevier.

SUMMERFIELD, W. C. 1969 On the trapping of wave energy by bottom topography. *Horace Lamb Centre Ocean Res., Flinders University Res.* Paper no. 20.